IEEE Photonics Journal
An IEEE Photonics Society Publication

Open Access

Terahertz Metalens for Multifocusing Bidirectional Arrangement in Different Dimensions

Volume 11, Number 1, February 2019

Jicheng Wang
Jing Ma
Zhenqiu Shu
Zheng-Da Hu
Xiaojun Wu

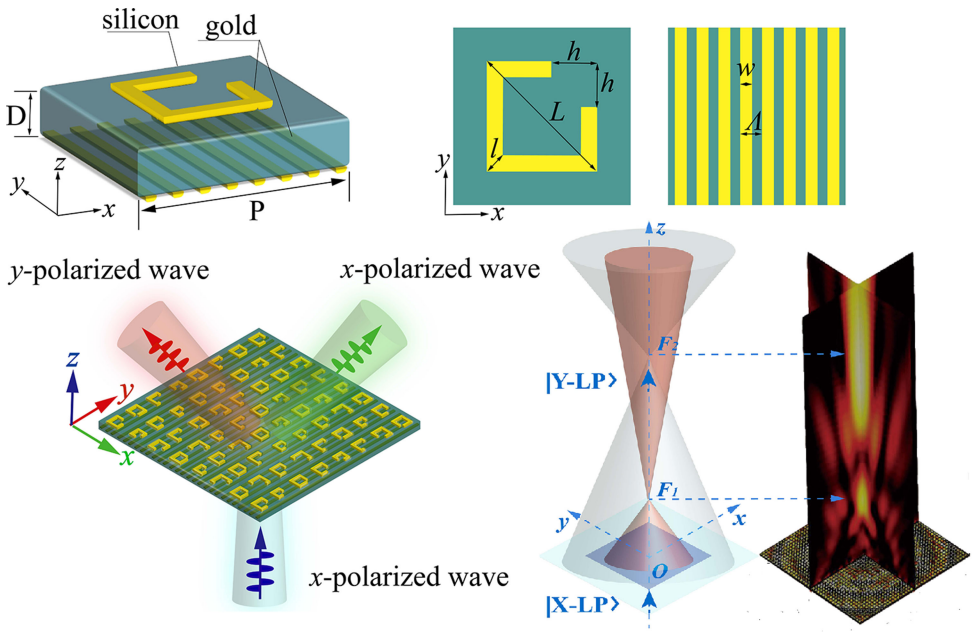

DOI: 10.1109/JPHOT.2019.2890903
1943-0655 © 2019 IEEE

Terahertz Metalens for Multifocusing Bidirectional Arrangement in Different Dimensions

Jicheng Wang [1,2] **Jing Ma,**[1] **Zhenqiu Shu** [2] **Zheng-Da Hu** [1] **and Xiaojun Wu** [2,3]

[1]School of Science, Jiangnan University, Wuxi 214122, China
[2]School of Computer Engineering, Jiangsu University of Technology, Changzhou 213001, China
[3]School of IoT Engineering, Jiangnan University, Wuxi 214122, China

DOI:10.1109/JPHOT.2019.2890903

Manuscript received December 3, 2018; revised December 28, 2018; accepted December 31, 2018. Date of current version October 18, 2019. This work was supported in part by the National Natural Science Foundation of China under Grant Nos. 11504139, 11504140, and 11811530052, in part by the China Postdoctoral Science Foundation under Grants 2017M611693 and 2018T110440, and in part by the Open Fund of State Key Laboratory of Millimeter Waves under Grant No. K201802. Corresponding author: Jicheng Wang (e-mail: jcwang@jiangnan.edu.cn).

Abstract: Metasurface lenses are typically investigated for a lot of characteristics, but the design method for conventional devices is comparatively simple in terms of controlling the quantity, position, and size of focal spots. Herein, ultra-thin-phase metasurface structures based on complementary square-split-ring (SSR) nanoantennas have been proposed to achieve terahertz (THz) optical metalenses with multidimensionality and multifocusing. The principle of beam propagation and efficient transmission can be effectively explained through the Fabry–Pérot resonance mode. The THz metalens can efficiently transfer linear cross-polarization under the effects of gratings in the incident plane. By locally tailoring edge lengths and opening the angles of the split rings, full control over abrupt phase changes can be achieved. Two symmetrically distributed parallel focal spots and two vertical focal spots with arbitrary distance can be obtained by arranging the SSR units on the metalenses. Furthermore, we apply the concept of a partitioned-phase mode to realize a double-focusing metalens in the longitudinal direction, which provides a flexible and convenient method to achieve the desired focusing properties. The simulation results are expected to pave the way for practical use of metasurfaces in optical holography, optical-information coding, and parallel-particle trapping.

Index Terms: Multifocusing metalens, Fabry-Pérot-like resonance, phase shift, nanoantenna, terahertz.

1. Introduction

Metamaterials based on new types of artificially engineered optical devices have been achieved through the manipulation of electromagnetic (EM) polarization, with applications to optical vortices [1], optical focusing [2], high-resolution holography [3], [4], and quarter-wave plates [5]. Metasurfaces, which are two-dimensional (2D) counterparts to metamaterials comprising individual structures, have attracted great interests in recent years owing to their unique properties and simple fabrication [6]. Some metasurfaces rely on subwavelength nanoantennas that play a significant role

in creating arbitrary phase profiles across 2π for cross-polarized scattered light and in ensuring uniform amplitudes [7]. Each nanoantenna acts as a unit cell and realizes simple modulation of optical properties based on the fine design of both the geometrical parameters and rotation angles; for example, engineering the phase of polarized light with high accuracy and high polarization-conversion efficiency is an application to which metalenses are perfectly suited.

Conventional lenses—such as Fresnel, and Luneburg lenses—are based on the reflection and refraction of light at the interface of the medium, as well as the phase accumulation along the optical path during wave propagation in the medium to manipulate the wave front [8], [9]. Moreover, the thicknesses of these conventional optical components are generally greater than or comparable to the operating wavelength owing to optical properties such as the refractive index and anisotropy of natural materials. Recently, optical metalenses have become indispensable tools under comprehensive study toward more integrated, planar, and precise ways to operate the incidence [10]–[12]. Researchers have been fascinated by the various principles and technologies going into the design of metalenses with unusual functions.

To our knowledge, focusing metalenses on basic substrates have many characteristics. First, many studies have been devoted to the design of multifocal metalenses, which are designed to have different focal lengths in the longitudinal or transverse directions [13]–[16]. Additionally, metalenses with many focusing spots have been proposed mainly based on the phase-retrieval algorithm and the parabolic-phase-variation algorithm [11], [17]–[19]. Few investigations have attempted to simultaneously design multidimensional and multifocal metalenses based on the holistic and partitioned modes [20]–[22].

In this study, we propose a complementary square split ring (SSR) nanostructure to realize a multidimensional ultrathin flat metalens with multifocusing along the horizontal and longitudinal directions. The unit structure is composed of the SSR nanoantennas, a subwavelength grating layer and a silicon substrate. The polarization state of the incident wave can be converted into a cross-polarization wave. Firstly, we show the multifocusing metalenses, aiming to implement the lenses with focal spots of arbitrary number, position, and size along the horizontal and longitudinal directions. Using mode partitioning and Parancharatnam–Berry (PB) phase modulation, we then arrange the SSR units selected into an annular-like array to construct multifocus metalenses; this array is simulated via finite-difference time-domain (FDTD) numerical computation. Such metalenses can more flexibly modify the quantity of foci arranged, as well as the process of ultrathin and integrated devices as compared with other metalenses.

2. Design and Methods

2.1 SSR-Shaped Nanoantennas

The basic unit nanostructure proposed is composed of two ultrathin metasurface layers, which are separated on the top (SSR-gold-nanoantennas) and the bottom (gold-grating) sides of a silicon substrate, as shown in Fig. 1(a). Uniform gold arrays and gold SSR nanoantennas can be fabricated on silicon substrate of a certain thickness using e-beam evaporation and e-beam lithography [23]. Here, the unit period P, width w and period Λ of the gold gratings, the silicon substrate thickness D, the thickness of the nanoantennas and the gratings d, and the nanoantenna width of diagonal line l are fixed whereas the peripheral diagonal values of square ring L and the incomplete length h at the ring gap are proposed to be the two degrees of freedom in the manipulation of EM polarization. Hence the transmission phase of cross-polarized light can be modulated and a series of desired units can be chosen accordingly. Remarkably, the $\pm 45^\circ$ orientations of the SSRs are selected to maximize the transmission amplitude of the polarized component [24], [25]. Numerical simulations of the transmission spectrum were performed by CST Microwave Studio in frequency domain. The x-polarization of the illumination is used to excite the configuration from gold gratings to SSR nanoantennas. For the y-polarized transmitted field, the almost equal transmission amplitudes and phase shifts (from 0 to 2π with $\pi/6$ intervals) of the twelve proposed SSR nanoantenna units under different parameters are shown in Fig. 1(b). Considering the actual thickness of silicon wafer and

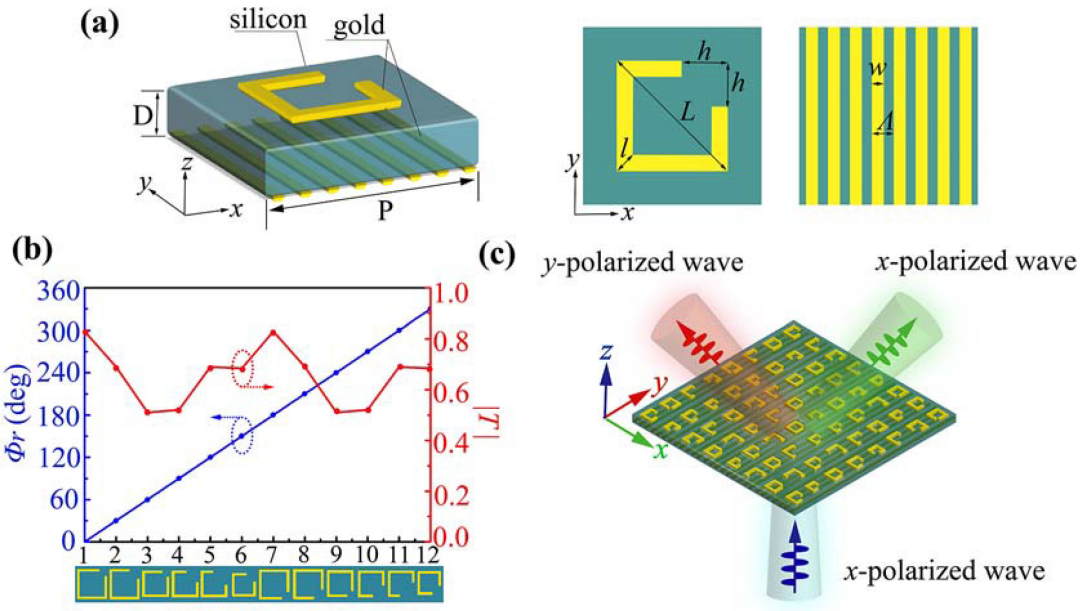

Fig. 1. (a) Schematic view of the SSR. (b) Simulated phase shifts and transmission amplitudes of the cross-polarized light from the individual SSRs under x-polarized normal incidence. (c) A diagram of the polarization wave transmission produced by a metasurface. The x-polarized wave incident from the grating layer. The transmitted wave includes high-intensity y-polarized light and weak-intensity co-polarized light.

combining with the Fabry-Pérot-like resonance matching condition (the theory will be introduced in Section 2.2), the thickness of silicon substrate can be determined. Then, invariable structural parameters can be further determined by setting initial parameters of SSR and optimizing the period of unit cell, thickness of silicon substrate and grating parameters in the simulation software. Due to gold is the reflective metal, and the interaction between the metal and the dielectric layers will excite surface plasmon polaritons (SPP) waves, which will lead to ohmic loss [26]–[28]. Therefore, we choose gold grating as a polarizer, which can effectively improve the transmission efficiency of cross-polarized light and suppress reflection and absorption.

For a fixed frequency of 0.86 THz, the unit-cell parameters are set as $P = 80\ \mu$m, $w = 4\ \mu$m, $\Lambda = 10\ \mu$m, $D = 25\ \mu$m, $d = 200$ nm, and $l = 8\ \mu$m. The first six SSRs have ide lengths of $L = 90$, 90, 80, 80, 80, and 70 μm, with corresponding incomplete lengths of $h = 20.3$, 24.6, 22.5, 36.7, 45.31, and 36.85 μm, respectively. The other six SSRs are mirror images of the first six SSR nanoantennas. The basic design schematic of a metalens is illustrated in Fig. 1(c). In agreement with focusing-theoretical analysis, 2D or 1D metalenses with convergent phase profiles are arranged to engineer a transmitted wavefront by employing the designed SSRs. Moreover, we discuss the numerically simulated cross- and co-polarized transmittances for normal incidence with the x-polarized light.

2.2 SSR Fabry-Pérot-Like Resonance

To demonstrate that the SSR nanoantennas retain high-efficiency functionality when transmitting the EM polarization, a scattering-process mode based on tracking the various Fabry–Pérot resonances is proposed [29]–[31] as shown in Fig. 2(a). Each of the metallic layers in the structure, i.e., gold gratings and nanoantennas, can be considered to be perfectly-matched and impedance-tuned surfaces. For each interface of the schematic, the transmission and refection coefficients of the cross-polarized wave can be denoted as t and r at interface 1 of the air-nanoantenna-silicon layer, and as t' and r' at interface 2 of the silicon-gratings layer. The incident wave E_σ with polarization

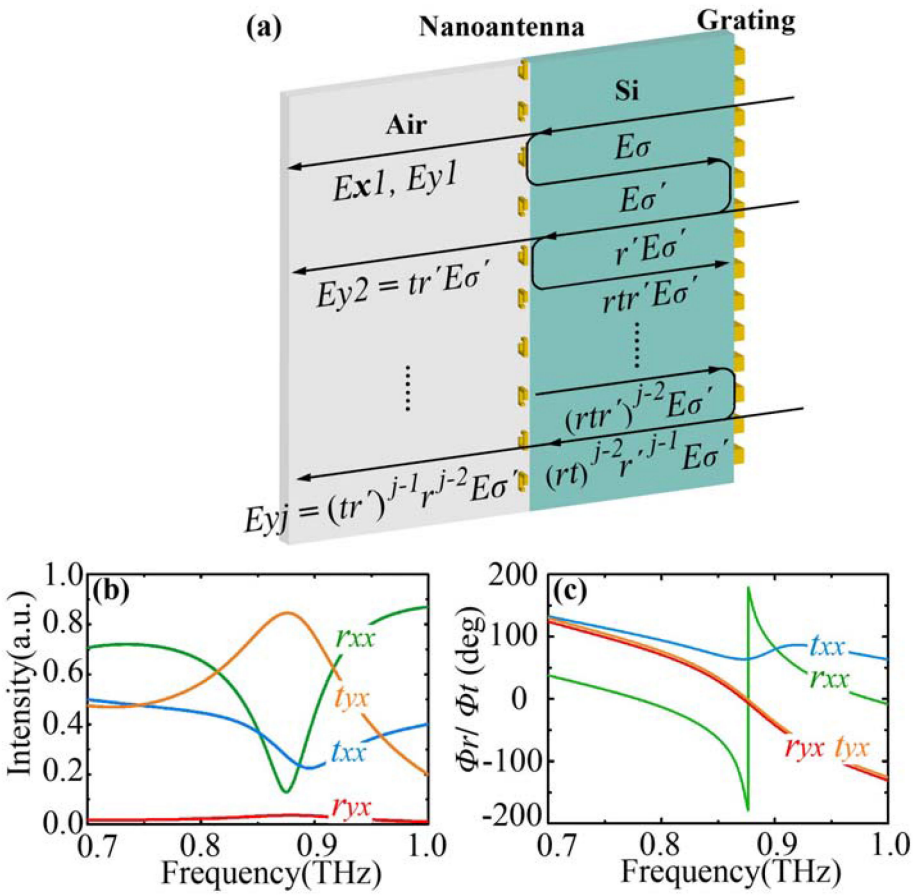

Fig. 2. (a) Schematic of multiple resonance in the Fabry–Pérot-like metasurface-polarization state under the cross-polarized transmission wave; reflected and transmitted amplitude (b) and phase spectra (c) of Co- (σ = x) and cross-polarized (σ' = y) light at 0.86-THz incidence.

($\sigma = x$) propagates from the gratings layer to structure; there are a total of two polarization components in the transmitted wave, i.e., x-polarized E_{x1} and y-polarized E_{y1}, $E_{\sigma'}$ denotes the lights reflected by interface 1. More significantly, the y-polarized wave can be reflected whereas the x-polarized wave can be transmitted almost entirely at interface 2 because the gratings are parallel to the *y*-direction. After multiple resonances, the final transmitted wave can be represented as E_{yj}, where *j* denotes the number of transmissions at interface 1. Ultimately, the sum, $\Sigma E_{y,}$ of the y-polarized component can be formed by the superposition of each E_{yi} and described as:

$$\sum_{j=1}^{j} E_y = E_{y1} + E_{y2} + \cdots + E_{yj}$$
$$= E_{y1} + \left[tr' + (tr')^2 r + \cdots + (tr')^{j-1} r^{j-2}\right] E_{\sigma'}. \quad (1)$$

Then the result can be simplified as $\Sigma E_y = E_1 + tE_{\sigma'} / (1 - r)$. Where parameter *r'* is equal to 1. Simultaneously, the optical Length of the Fabry-Pérot-Like resonator, i.e., the thickness D of silicon substrate, and the refractive index n of the silicon satisfy the resonance matching condition which is 2 nDF/c + $\triangle\psi$ = 2 mπ (m is an integer), where F and c are the frequency (0.86 THz), $\psi$is the is the sum of phase modulation of multiple interfaces. Then, using the unit cell with transmission phase equal to 0°, we simulated the reflection and transmission amplitude and phase spectra of

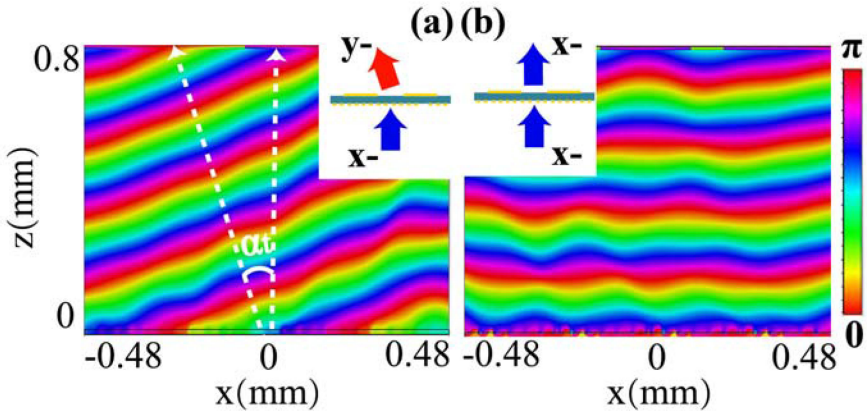

Fig. 3. The simulated phase profiles of transmitted field component E_y (a) and transmitted field component E_x (b) for the x-polarized normal illumination, demonstrating the wave front behind the converter.

co-($\sigma = x$) and cross-polarized ($\sigma' = y$) light at 0.86 THz with the theoretical expression (1), as shown in Fig. 2(a, b). For the individual interfaces, $r_{\sigma\sigma}$ $r_{\sigma'\sigma}$ and $t_{\sigma\sigma}$, $t_{\sigma'\sigma}$ denote the reflection and transmission coefficients. Between 0.82 and 0.9 THz, the cross-polarized transmission t_{yx} carries more than 80% of the incident power, whereas the co-polarized component t_{xx} is mostly below 20%. When the incident frequency is below 0.82 or higher than 0.9 THz, the co-polarized reflection, r_{xx}, is higher than 70%, and both the transmission and the cross-polarized reflection are simultaneously quite inefficient due to the limit of dielectric loss. Furthermore, for the co-polarized reflection, a novel phenomenon is observed at the excitation frequency where a phase break of π radians occurs, and the phase shift of the cross-polarized transmission is 0°, as shown in Fig. 2(b), representing a broadband and high-efficiency cross-polarization converter in transmission.

3. Results and Discussion

3.1 Anomalous Refraction Based on Twelve SSR Unit

A one-dimensional (1D) chain with 12 unit cells have been used to investigate the bending phenomenon for x-polarization in order to achieve the phase variation from 0 to 2π. A cross- polarization wave and a co-polarization wave are imposed along the interface of converter in the phase profiles of transmitted field, which have been described in Fig. 3; then, the deflection angle, α_t, can be obtained based on phase matching for cross- polarization wave. Under x-polarization-incidence, the deflection angle of α_t could be described by the generalized Snell's Law [10], [32]:

$$n_t \sin\alpha_t - n_i \sin\alpha_i = \frac{\lambda}{2\pi}\frac{d\Phi(x)}{dx}, \tag{2}$$

where α_i (=0) represents the normal incidence angle and n_i and n_t are the refractive index of the medium at the incident (silicon) and transmitted (air) sides. According to the transverse wave vector, $k = d\phi(x)/dx = 2\pi/(nP)$, where n is the number of units used by a converter and P is the unit period. Then, the deflection angle of α_t can be simplified as $\alpha_t = \sin^{-1}(\lambda/12P) = 21.1°$. From Fig. 3(a), we can notice that the simulated α_t is 21°, which is almost the same as the theoretical calculation (21.1°). As we mentioned before, the transmitted light includes not only high intensity y-polarization, but also extremely weak x-polarization. For the transmitted phase profile of x-polarization, as depicted in Fig. 3(b), compared with the incident plane wave, the phase distribution is almost unchanged. Furthermore, the distribution trend of the two transmitted fields is consistent with the phase, and the intensity of the transmitted field of x-polarized light is far less than that of the y-polarized light, which is almost negligible [33].

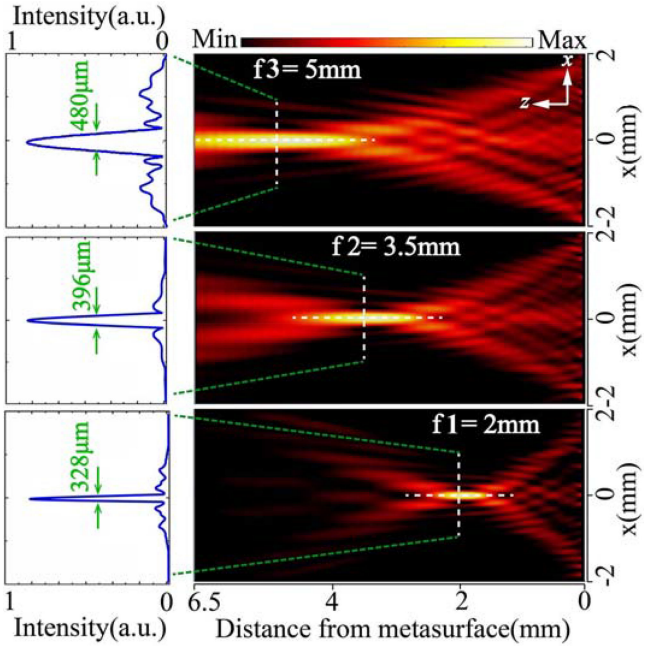

Fig. 4. The simulated results of the 1D single-point metalens. Different focal distribution of the metalens. The left illustrations correspond to the radial electric field intensity profiles on the initial plane.

3.2 1D Single-Focus Metalenses With Varied Focal Lengths

Here, some high-performance THz devices based on proper arrangement of SSR metalenses are proposed, including the 1D-single focusing metalenses and the 1D-double focusing metalenses in the horizontal or longitudinal directions. For plane-wave incidence, each nanoantenna needs to be arranged to interfere constructively at the predetermined focal spot in the transmission field. The optimization procedure for the SSR metalens has been numerically analyzed through MATLAB based on the principle of equal optical paths and PB phase modulation [34]–[36]. According to these principles, for a 1D single-point focusing metalens with a definite focal length *f*, the spherical phase profile can be expressed as

$$\varphi(x) = \frac{2\pi}{\lambda}\left(\sqrt{f^2 + x^2} - f\right) - 2m\pi, \tag{3}$$

where λ is the incident wavelength corresponding to the frequency at 0.86 THz and m is an integer selected to guarantee that $\phi(x)$ can be obtained between 0 and 2π.

Firstly, to investigate the basic performance of the SSR metalens, we have designed a series of 1D single-point-focusing metalenses with variable focal length and phase distribution according to (3). As shown in Fig. 4, each metalens is composed of 61 units and the preset focal lengths are $f = 2$, 3.5, and 5 mm, respectively. It can be shown that the focal-length tenability is flexible and that the longitudinal profiles of the focused light are perfect. The focal positions of the simulation are slightly different from the preset theoretical values, which may be due to the difference between the numerical-simulation model and the phase-shift-distribution equation. We can see that the full width at half maximum (FWHM) of the foci are 328, 396, and 480 μm in the cross-polarized electric field, along with the increase of the focal length, which demonstrates that these proposed 1D single metalenses offer high performance. Considering the principle of focus formation, all phase profiles for the three metalenses are drawn by the asteroid curve depicted in Fig. 5(a). In each of the 61 arrays, the transmission-phase shift is marked by the simple dot and, through it, the relative phase values need to be analogous and approximately equal to the twelve units with preset fixed phase

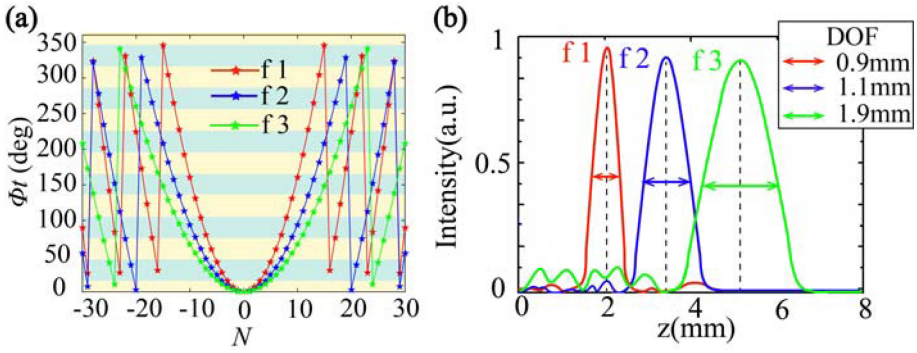

Fig. 5. The phase profiles (a) and the axial-intensity distributions extracted from the center line (b) for three preset focal lengths (f = 2, 3.5, and 5 mm) according to (3).

shift. With the same number of arrays, the shorter the focal length is, the more diversified and accurate the phase shifts are chosen theoretically. According to the simulation, the depths of focus (DOFs) along the *z*-axis of the foci are designed to be 0.9, 1.1, and 1.9 mm for the three designed metalenses, respectively, as depicted in Fig. 5(b). According to the numerical aperture NA = sin [$\tan^{-1}$(D/2f)], the NA of the lenses we designed are about 0.2, mainly because of the large focal length, which reduces the NA to a certain extent. We also observed that the DOFs and transmission intensity continuously decrease as the focal length is gradually stretched. Here, we utilize a key factor in the practical design of metalenses, focusing energy efficiency, to evaluate the focusing results. It can be defined as the ratio of the energy at the foci to the total energy of the incident wave [37]. The focusing energy efficiency of the corresponding 1D single-focus metalens with f3 = 5 mm can be calculated using CST software and MATLAB, which is 20.7% at 0.86 THz. Energy diffusion at the foci edge is also an important issue to be considered in the design of metalenses Of these phenomena, implementing real-time optical morphological transforms of focal points and improving focusing properties can be achieved through a convertible focal length.

3.3 Bidirectional 1D Double-Foci Metalenses

To gain insight into multifocusing characteristics, two novel 1D-metalenses with multiple parallel and vertical foci are established in this subsection. Firstly, we built two 1D-metalenses model to control the phase distribution based on the arrangement of horizontal and longitudinal double-focus, as illustrated in Fig. 6(a, b). The distance between the two focal spots can be denoted as 2d, the optical paths from the two focal points to any point on the metasurface can be expressed as $r_1 = [f2 + (d + x)^2]^{1/2}$ and $r_2 = [f2 + (d - x)^2]^{1/2}$ for horizontal double-focusing, and as $r1 = [x^2 + (f - d)^2]^{1/2}$ and $r_2 = [x^2 + (f + d)^2]^{1/2}$ for longitudinal double- focusing. Thus, the equation of a plane wave superimposed at the reference point (x, 0) is

$$\vec{E} = \vec{E}_1 + \vec{E}_2 = \frac{1}{r_1}\exp(\vec{j}\vec{k}r_1)\hat{e}_1 + \frac{1}{r_2}\exp(\vec{j}\vec{k}r_2)\hat{e}_2. \tag{4}$$

Light refraction with a varying-phase discontinuity of ϕ(x) can be simultaneous simplified to give:

$$\tan\varphi(x) = \frac{(1/r_1)\sin kr_1 + (1/r_2)\sin kr_2}{(1/r_1)\cos kr_1 + (1/r_2)\cos kr_2}. \tag{5}$$

The effects of optical paths and wave equations can be analyzed with geometrical optics and physical optics theories, they can modulate transmitted phase of wavefront effectively. Then combining focal lengths, foci distance d, optical path difference from x position to two foci and phase distribution of target foci, the transmitted phase value at any position on metasurface can be deduced. Therefore, we can obtain the specific values of phase shifts for the corresponding nanoantennas,

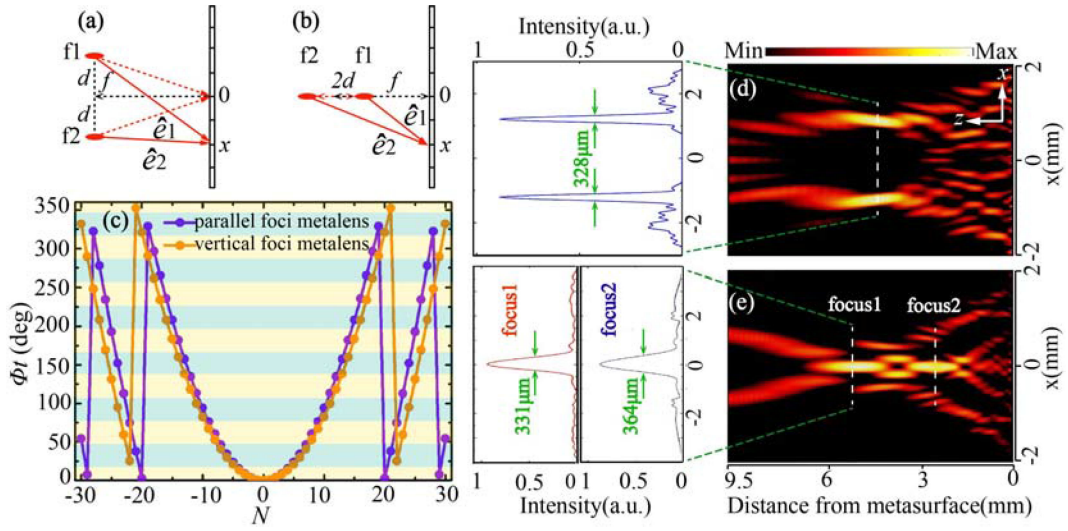

Fig. 6. The geometrical interpretation of beam propagation (a, b), the phase profiles (c) and the simulation-field-intensity distributions of 1D double-focus metalenses in the horizontal (d) and longitudinal directions (e).

and the concrete positions of the relative units can be determined through the foci approximation. The phase profiles for the parallel double-focus metalens and vertical double focus metalens are drawn by the different color curve depicted in Fig. 6(c). The electric-field distribution of a designed parallel double-focus metalens with f = 4 mm and distance 2d = 3.5 mm is shown in Fig. 6(d). When the metasurface is illuminated using a 0.86-THz x-polarization incidence, the patterns of the foci have a FWHM of 300 μm and a transmission ratio of approximately 0.8. We can conclude that the distinctions between the two focusing characteristics are all very slight. Additionally, the transmission-electric-field distribution of the designed metalens with vertical double foci (focal lengths f1 = 6 mm and f2 = 2.5 mm, distance 2d = 3.5 mm) is displayed in Fig. 6(e). For comparison, focus 1 has the smallest FWHM and the maximum transmission intensity.

3.4 2D Single-Focus Metalens

Generally speaking, 1D multifocal metalenses are not yet suitable for practical applications. A set of SSR nanoantennas are therefore selected to build 2D multifocal metalenses based on the calculated phase distribution in CST. To validate the focusing capability of such metalenses, 31 $\times$ 31 preset nanoantennas are arranged on a flat surface and the phase distribution is exhibited in Fig. 7(a). In the manner currently designed, the electric-field distribution of a cross-polarized wave is the main research object using x-polarized wave excitation. Furthermore, to achieve the maximum density and reduce interference between adjacent units, the optical-path difference between two adjacent units should be greater than the period P in the radial direction. Fig. 7(b) shows the intensity distributions, $|E_y|^2$, in the x-z and y-z planes of the metalens with $f = 2.5$ mm; the simulated result of the y-polarized field distribution on the respective focal plane (x-y plane) is shown in Fig. 7(c). The diameter of the focus is estimated to be about 350 μm from the FWHM in Fig. 7(c), and the intensity of focusing is about 80%. The 1D and 2D structures simultaneously offer good focusing effects, implying the capability-independence of the designed metalens.

3.5 2D Double-Foci Metalens in the Longitudinal Direction

We have found an alternative to designing 2D double-focusing metalenses based on the partitioned mode in the longitudinal direction, thereby offering a novel methodology to develop multifocal

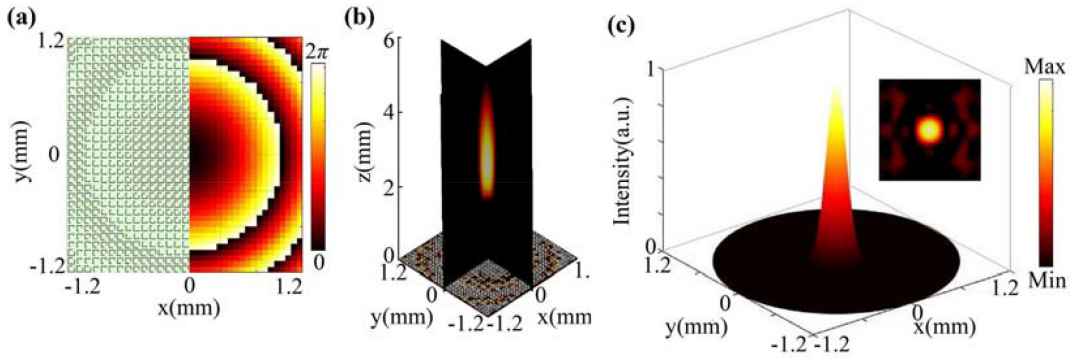

Fig. 7. (a) Design of a 2D single-focus metalens based on the SSR array. The distribution of the planar phase and the twelve basic units arranged for the simulation model considering (3) are shown. (b) Simulated $|Ey|^2$ distributions on both the x-z and y-z planes at the cross-polarized field when the metasurface is illuminated by an x-polarized normally incident wave. (c) The intensity distribution for a single-spot focusing plane.

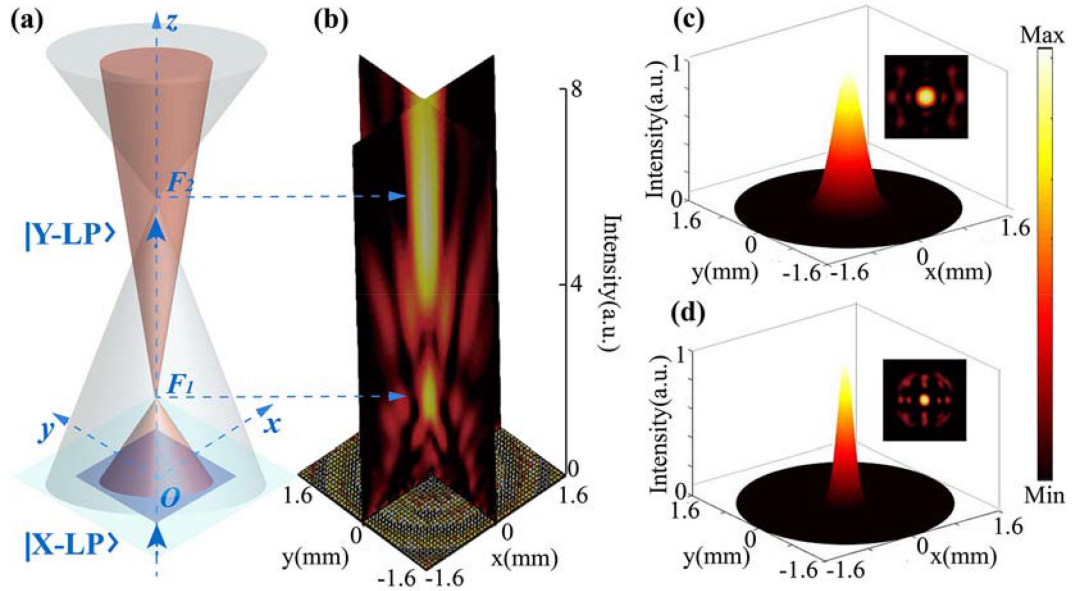

Fig. 8. (a) Schematic of the focusing formation of the 2D double-focus metalens based on the partitioned mode in which the metasurface is illuminated by an x-polarized normally incident wave. Two virtual focal points exist in the virtual focal planes corresponding to the electric-field distribution of the double-focus in figure (b), where |X-LP> denotes the incident x-linear polarization wave and |Y-LP> denotes the transmitted y-linear polarization wave. (b) Simulated $|Ey|^2$ distributions on both the x-z and y-z planes at the cross-polarized field when the metasurface is illuminated by an x-polarized normally incident wave. (c, d) The intensity distribution for the double-spot focusing plane.

metalenses with cross-polarization states on the focal planes; this means that the SSR nanoantenna arrays are partitioned into two concentric regions through the interference of numerous transmitted diffraction beams. As illustrated in Figs. 8(a, b), the whole metasurface consists of 41 $\times$ 41 nanostructures and the inner region has 21 $\times$ 21 units, thereby ensuring that the two regions have almost the same area. Hence, the two parts of the metalens can be irradiated equally by normal incidence and receive the same luminous flux. In order to construct a spherical phase profile, the relationship

determined by (3) can be expressed in more detail as follows:

$$\varphi(r) = \begin{cases} \frac{2\pi}{\lambda}\left(\sqrt{{f_1}^2 + r^2} - f_1\right), 0 \le r \le r_1 \\ \frac{2\pi}{\lambda}\left(\sqrt{{f_2}^2 + r^2} - f_2\right), r_1 \le r \le r_2 \end{cases}, \tag{6}$$

where $r = (x^2 + y^2)^{1/2}$ is the optical path from an arbitrary point (x, y) to the original point; r_1 and r_2 are the outermost ring diameters of two regions, respectively; the inner region is used to achieve the first focus with $f_1 = 2$ mm, and the outer region is used to achieve the second focus with $f_2 = 6$ mm. The focusing intensities and y-polarized-field distributions on the respective focal planes (x-y planes) are shown in Figs. 8(c, d) for the x-polarized incidence. By contrast, the intensities and qualities of all foci are almost equal. This clearly reveals that the diameter of the first focal spot is 370 μm while that of the second is twice that of the first. In addition, the number of units corresponding to each focus point can be changed to improve NA and to change the intensity ratio of the bifocal point on the premise that the size of the lens remains unchanged. This demonstrates that an alternative to modulating the preset parameters (e.g., focal length and bifocal distance) based on the principle of equal optical paths is possible. The previous theoretical analysis can be used in the generation of novel multifocal metalenses.

4. Conclusions

In summary, we have proposed a series of multidimensional and multifocal metalenses consisting of twelve gold SSR nanoantennas and gold gratings used for polarization conversion. For the normal incidence of x-polarized light with a fixed frequency in the terahertz region, the simulated results of the constructed chain double-focusing with the focal positions along the horizontal and longitudinal directions agree well with theoretical expectations and have excellent focusing features. Furthermore, a comparison of chain-like lenses and planar lenses for multifocal imaging has been made to facilitate the development of metasurface devices toward integration and practical applications. The partitioned-mode approach provides a flexible design for realizing a multifocusing metalens, which would open a new avenue for the THz-field-modulated device.

References

[1] P. Genevet *et al.*, "Ultra-thin plasmonic optical vortex plate based on phase discontinuities," *Appl. Phys. Lett.*, vol. 100, no. 1, Jan. 2012, Art. no. 013101.

[2] X. Z. Chen *et al.*, "Longitudinal multifoci metalens for circularly polarized light," *Adv. Opt. Mater.*, vol. 3, no. 9, pp. 1201–1206, May 2015.

[3] S. Larouche, Y. J. Tsai, T. Tyler, N. M. Jokerst, and D. R. Smith, "Infrared metamaterial phase holograms," *Nature Mater.*, vol. 11, no. 5, pp. 450–454, May 2012.

[4] J. Burch, D. D. Wen, X. Z. Chen, and A. D. Falco, "Conformable holographic metasurfaces," *Sci. Rep.*, vol. 7, no. 1, p. 4520, Jul. 2017.

[5] N. Yu, F. Aieta, P. Geneve, M. A. Kats, Z. Gaburro, and F. Capasso, "A broadband, background-free quarter-wave plate based on plasmonic metasurfaces," *Nano Lett.*, vol. 12, no. 12, pp. 6328–6333, Nov. 2012.

[6] N. Yu and F. Capasso, "Flat optics with designer metasurfaces," *Nature Mater.*, vol. 13, no. 2, pp. 139–150, Jan. 2014.

[7] A. Forouzmand, S. Tao, S. Jafar-Zanjani, J. Cheng, M. M. Salary, and H. Mosallaei, "Double split-loop resonators as building blocks of metasurfaces for light manipulation: Bending, focusing, and flat-top generation," *J. Opt. Soc. Amer. B*, vol. 33, no. 7, pp. 1411–1420, Jul. 2016.

[8] Q. Yang *et al.*, "Efficient flat metasurface lens for terahertz imaging," *Opt. Exp.*, vol. 22, no. 21, pp. 25931–25939, Oct. 2014.

[9] F. Shen *et al.*, "Polarization-independent longitudinal multifocusing metalens," *Opt. Exp.*, vol. 23, no. 23, pp. 29855–29866, Nov. 2015.

[10] J. P. B. Mueller, N. A. Rubin, R. C. Devlin, B. Groever, and F. Capasso, "Metasurface polarization optics: Independent phase control of arbitrary orthogonal states of polarization," *Phys. Rev. Lett.*, vol. 118, no. 11, Mar. 2017, Art. no. 113901.

[11] M. Kang, T. Feng, H. T. Wang, and J. Li, "Wave front engineering from an array of thin aperture antennas," *Opt. Exp.*, vol. 20, no. 14, pp. 15882–15890, Jul. 2012.

[12] H. Shao, C. Chen, J. Wang, L. Pan, and T. Sang, "Metalenses based on the non-parallel double-slit arrays," *J. Phy. D, Appl. Phys.*, vol. 50, no. 38, Jul. 2017, Art. no. 384001.

[13] G. P. De, C. Dorronsoro, and S. Marcos, "Multiple zone multifocal phase designs," *Opt. Lett.*, vol. 38, no. 18, pp. 3526–3529, Sep. 2013.

[14] P. J. Valle and M. P. Gagigal, "Analytic design of multiple-axis, multifocal diffractive lenses," *Opt. Lett.*, vol. 37, no. 6, pp. 1121–1123, Mar. 2012.
[15] D. D. Wen, F. Y. Yue, M. Ardron, and X. Z. Chen, "Multifunctional metasurface lens for imaging and Fourier transform," *Sci. Rep.*, vol. 6, Jun. 2016, Art. no. 27628.
[16] Y. J. Bao, Q. Jiang, Y. M. Kang, X. Zhu, and Z. Y. Fang, "Enhanced optical performance of multifocal metalens with conic shapes," *Light-Sci. Appl.*, vol. 6, no. 10, Oct. 2017, Art. no. e17071.
[17] Q. Wang, X. Q. Zhang, Y. H. Xu, and W. L. Zhang, "A broadband metasurface-based terahertz flat-lens array," *Adv. Opt. Mater.*, vol. 3, no. 6, pp. 779–785, Feb. 2015.
[18] J. W. He, J. S. Ye, X. K. Wang, Q. Kan, and Y. Zhang, "A broadband terahertz ultrathin multi-focus lens," *Sci. Rep.*, vol. 6, Jun. 2016, Art. no. 28800.
[19] X. Z. Chen, Y. Zhang, L. L. Huang, and S. Zhang, "Ultrathin metasurface laser beam shaper," *Adv. Opt. Mater.*, vol. 2, no. 10, pp. 978–982, Jun. 2014.
[20] M. Y. Li, W. Y. Li, H. Y. Li, Y. C. Zhu, and Y. T. Yu, "Controllable design of superoscillatory lenses with multiple subdiffraction-limit foci," *Sci. Rep.*, vol. 7, no. 1, p. 1335, Dec. 2017.
[21] S. Mei *et al.*, "Flat helical nanosieves," *Adv. Funct. Mater.*, vol. 26, no. 29, pp. 5255–5262, May 2016.
[22] M. Hashemi, A. Moazami, M. Naserpour, and C. J. Zapata-Rodríguez, "A broadband multifocal metalens in the terahertz frequency range," *Opt. Commun.*, vol. 370, pp. 306–310, Jul. 2016.
[23] X. X. Wang *et al.*, "Theoretical investigation of subwavelength structure fabrication based on multi-exposure surface plasmon interference lithography," *Results Phys.*, vol. 12, pp. 732–737, 2019.
[24] L. Liu *et al.*, "Broadband metasurfaces with simultaneous control of phase and amplitude," *Adv. Mater.*, vol. 26, no. 29, pp. 5031–5036, Aug. 2014.
[25] S. Sakaguchi and N. Sugimoto, "Transmission properties of multilayer films composed of magneto-optical and dielectric materials," *J. Light. Technol.*, vol. 17, no. 6, pp. 1087–1092, Jul. 2002.
[26] J. Chen *et al.*, "Surface-plasmon-polaritons-assisted enhanced magnetic response at optical frequencies in metamaterials," *IEEE Photon. J.*, vol. 8, Feb. 2016, Art. no. 4800107.
[27] C. Liang *et al.*, "Tunable triple-band graphene refractive index sensor with good angle-polarization tolerance," *Opt. Commun.*, vol. 436, pp. 57–62, Apr. 2019.
[28] C. Cen *et al.*, "Plasmonic absorption characteristics based on dumbbell-shaped graphene metamaterial arrays," *Physica E*, vol. 103, pp. 93–98, Feb. 2018.
[29] H. J. W. M. Hoekstra, G. J. M. Krijnen, and P. V. Lambeck, "Efficient interface conditions for the finite difference beam propagation method," *J. Light. Technol.*, vol. 10, no. 10, pp. 1352–1355, Nov. 2017.
[30] Z. Liu, G. Liu, K. Huang, Y. Chen, Y. Hu, and X. Zhang, "Enhanced optical transmission of a continuous metal film with double metal cylinder arrays," *IEEE Photon. Technol. Lett.*, vol. 25, no. 12, pp. 1157–1160, Jun. 2013.
[31] J. Chen *et al.*, "Optical magnetic field enhancement via coupling magnetic plasmons to optical cavity modes," *IEEE Photon. Technol. Lett.*, vol. 28, no. 14, pp. 1529–1532, Jul. 2016.
[32] F. Aieta, P. Genevet, N. Yu, M. A. Kats, Z. Gaburro, and F. Capasso, "Out-of-plane reflection and refraction of light by anisotropic optical antenna metasurfaces with phase discontinuities," *Nano Lett.*, vol. 12, no. 3, pp. 1702–1706, Feb. 2012.
[33] Y. Yuan, K. Zhang, X. M. Ding, B. Ratni, S. N. Burokur, and Q. Wu, "Complementary transmissive ultra-thin meta-deflectors for broadband polarization-independent refractions in the microwave region," *Photon. Res.*, vol. 7, no. 1, pp. 80–88, 2019.
[34] Y. G. Ke, W. X. Shu, H. L. Luo, S. C. Wen, and D. Y. Fan, "Method for arbitrary phase transformation by a slab based on transformation optics and the principle of equal optical path," *J. Eur. Opt. Soc.-Rapid*, vol. 7, Jan. 2012, Art. no. 12013.
[35] E. Hasman, V. Kleiner, G. Biener, and A. Niv, "Polarization dependent focusing lens by use of quantized Pancharatnam–Berry phase diffractive optics," *Appl. Phys. Lett.*, vol. 82, no. 3, pp. 328–330, Jan. 2003.
[36] S. M. Choudhury, A. Shaltout, A. V. Kildishev, V. M. Shalaev, and A. Boltasseva, "Experimental realization of color hologram using pancharatnam-berry phase manipulating metasurface," in *Proc. Conf. Lasers Electro-Opt.*, Jan. 2016, Paper FF1D.8.
[37] K. Zhang *et al.*, "Phase-engineered metalenses to generate converging and non-diffractive vortex beam carrying orbital angular momentum in microwave region," *Opt. Exp.*, vol. 26, no. 2, pp. 1351–1360, 2018.